Nanoscale Copper–Tin Dioxide Interfaces for Efficient CO2 Electroreduction to Formic Acid and Formate at High Rates

ChemSusChem

Research Article
doi.org/10.1002/cssc.202501686

Chemistry Europe
European Chemical Societies Publishing

www.chemsuschem.org

Nanoscale Copper–Tin Dioxide Interfaces for Efficient CO_2 Electroreduction to Formic Acid and Formate at High Rates

Lan Huang,* Felicia Di Costola, Marco Allione, Stefano Bianco, Adriano Sacco, Candido F. Pirri, and Juqin Zeng*

This study reports highly selective and stable electrocatalysts consisting of Cu and Sn for efficient reduction of CO_2 to formate ($HCOO^-$) and formic acid (HCOOH). The copper–tin dioxide catalyst (CuSn) is prepared through a one-pot microwave-assisted solvothermal method. Different samples are obtained by varying Cu-to-Sn atomic ratios from 4 to 1. When Sn content is low, the CuSn sample shows a main crystalline phase of cuprous oxide (Cu_2O), with low amounts of surface CuO and SnO_2 species. An increase in Sn percentage leads to the appearance of the crystalline phase of metallic Cu and SnO_2, which becomes dominant for the sample with the highest Sn content. During CO_2 electrolysis, the optimal CuSn material shows a faradaic efficiency (FE) for $HCOO^-$ greater than 90% at $-200\,mA\,cm^{-2}$ in a flow cell with alkaline electrolyte. It also performs well under acidic condition (pH 3) to produce HCOOH with an FE of 70% at the same current density. A long-term test is carried out in 1 M KOH at $-100\,mA\,cm^{-2}$ for over 20 h, showing good retention in FE_{HCOO-}. This study highlights the potential of implementing low-cost catalysts for CO_2 conversion at an industrial scale.

1. Introduction

In recent decades, the overexploitation and intense use of fossil fuels have led to rapid depletion of fuel availability and increased CO_2 emissions. Electrochemical conversion of CO_2 to produce high-value fuels and chemicals is a promising pathway to mitigate the CO_2-related greenhouse effect and promote economic sustainability.[1–6] Among many products, formic acid (HCOOH) is of high interest as a convenient hydrogen storage medium via reversible CO_2 hydrogenation.[7,8]

At present, various metals such as tin (Sn),[9,10] indium (In),[11] bismuth (Bi),[12,13] cobalt (Co),[14] and palladium (Pd)[15] have been investigated as catalysts to produce HCOOH or formate ($HCOO^-$) from electrochemical CO_2 reduction reaction (CO_2RR). Among these metals, Sn electrocatalysts have attracted particular attention since it is a noncritically raw metal and have exhibited excellent selectivity for CO_2-to-$HCOO^-$ (or HCOOH) conversion.[16,17] However, industrial deployment remains limited by the high overpotentials required to sustain high current densities with good faradaic efficiencies, as well as by the low stability of Sn-based catalysts.[18] Alloying Sn with other metals could be a promising strategy. It is well known that Cu is effective in activating CO_2 molecule and uniquely converts it into hydrocarbon products,[19–22] while its selectivity for $HCOO^-$ or HCOOH is very limited. Combining Sn with Cu could take advantage of both Sn and Cu, maintaining excellent selectivity for $HCOO^-$ (or HCOOH) at relatively low overpotentials and improved stability. Some works have been reported to deliver an excellent CO_2-to-$HCOO^-$ conversion by tuning the composition or structure of the CuSn bimetallic catalysts.[23–29] Wang et al.[27] reported that the excellent activity in electrocatalytic reduction of CO_2 to $HCOO^-$ is ascribed to the abundant Cu/SnO_2 interfaces in the heterostructure, by reducing the reaction free energies for the formation of $HCOO^-$ species. Lei et al.[28] achieved effective performance for the electrochemical CO_2 reduction to $HCOO^-$ through reconstruction of CuS/SnO_2-S nanoparticles to Cu/Sn/$Cu_{6.26}Sn_5$ nanowires. Gunji et al.[29] reported that carbon-black-supported Cu_6Sn_5 core–shell nanoparticles give 65% faradaic efficiency for $HCOO^-$ at ≈−0.6 V, superior to Cu or Sn alone, highlighting the importance of intermetallic-core/oxide-shell synergy. However, most of the previously reported electrocatalysts still have limitations for $HCOO^-$ generation via CO_2RR, such as complicated preparation methods and limited working conditions such as low current densities and narrow potential windows.

In this regard, we present a facile one-pot microwave-assisted method for the synthesis of CuSn-based nanocomposites for efficient CO_2RR. The optimal CuSn material exhibits excellent selectivity and good stability for $HCOO^-$ and HCOOH production

L. Huang, F. Di Costola, A. Sacco, C. F. Pirri, J. Zeng
Centre for Sustainable Future Technologies (CSFT)
Istituto Italiano di Tecnologia – IIT
Via Livorno 60, 10144 Turin, Italy
E-mail: lan.huang@iit.it
juqin.zeng@polito.it

L. Huang, F. Di Costola, M. Allione, S. Bianco, C. F. Pirri, J. Zeng
Department of Applied Science and Technology (DISAT)
Politecnico di Torino
Corso Duca degli Abruzzi 24, 10129 Turin, Italy

Supporting information for this article is available on the WWW under https://doi.org/10.1002/cssc.202501686

across a wide range of current densities in alkaline and acidic electrolytes, respectively.

2. Experimental Section

2.1. Chemicals

Copper (II) acetate hydrate [Cu $(OAc)_2 \cdot xH_2O$], tin sulfate ($SnSO_4$), ethylene glycol, potassium hydroxide (KOH), and potassium sulfate (K_2SO_4) of analytical grade were purchased from Merck. All chemicals were used as received. Deionized water was supplied by MyMilli-Q Lab Water Systems (18.2 MΩ cm, 25 °C).

2.2. Synthesis

The preparation of CuSn bimetallic catalyst is schematically represented in **Scheme 1**, through a microwave-assisted process. Initially, 40 mL ethylene glycol (EG) and 5 mL H_2O were mixed. 2.5 mmol Cu $(OAc)_2 \cdot xH_2O$ and 2.5 mmol $SnSO_4$ were added to the mixture and stirred for 1 h until the complete dissolution of the salts. The solution was then transferred into a Teflon vessel and irradiated for 2 min ($T_{max} = 220$ °C, $Power_{max} = 900$ W). After cooling down to 60 °C, the precipitates were washed twice with water and once with ethanol, each time centrifuged at 4900 rpm for 10 min, and then dried under vacuum. The obtained catalyst prepared was named Cu_5Sn_5. The nanocomposites with different atomic ratios of Cu-to-Sn were prepared by changing the ratio of Cu and Sn precursors (8:2 and 7:3), and the total mole of the metal salts was kept at 5 mmol for each synthesis. The synthesized catalyst with only Cu $(OAc)_2 \cdot xH_2O$ precursor was denoted as Cu_2O catalyst.

2.3. Physicochemical Characterization

X-ray diffraction (XRD) was performed in Bragg–Brentano symmetric geometry by using a PANalytical X'Pert Pro instrument (CuKa radiation, 40 kV and 30 mA) equipped with an X'Celerator detector.

Field emission scanning electron microscopy (FESEM, ZEISS Auriga) was used to evaluate the morphology of the materials. For transmission electron microscopy (TEM) analysis, the sample was deposited on a commercial lacey carbon film suspended on an Au grid (Ted Pella Inc., USA) and analyzed in a Talos F200X TEM operated at its maximum acceleration voltage of 200 kV, equipped with an in-column energy-dispersive X-ray (EDX) detector for elemental analysis.

The actual atomic ratios of Cu to Sn in the CuSn samples were determined by inductively coupled plasma–optical emission spectrometry (ICP–OES) analysis.

Raman spectra were acquired on solid powders deposited on a microscope slide by means of a Renishaw InVia Reflex micro-Raman spectrometer, equipped with a cooled Charge Coupled Device (CCD) camera. The light source was a laser diode ($\lambda ex = 514.5$ nm) with power lower than 10 mW, and sample inspection occurred through a microscope objective (50×), in backscattering light collection conditions.

2.4. Preparation of Electrodes

Herein, a drop-casting method was used to fabricate the electrodes. Typically, 7.5 mg catalyst, 450 μL isopropanol, and 80 μL Nafion117 solution were sonicated for 20 min until a uniform slurry was obtained. Then, the slurry was coated onto a carbon gas diffusion layer (GDL; SI-GRACET 28BC, SGL Technologies) substrate. The obtained electrode was dried at room temperature overnight in the air. The mass loading of each catalyst was ≈1.67 mg cm^{-2}.

2.5. Electrochemical CO_2RR Tests

The CO_2RR experiments were performed on the Biologic potentiostat in a commercial flow cell (ElectroCell A/S) at room temperature. All tests were conducted in a chronopotentiometry (CP) mode. The cell configuration was composed of three chambers and three electrodes, as shown in Figure S1, Supporting Information. An anion exchange membrane (Sustainion X37-50 Grade RT, Dioxide Materials) divided the cell into anodic and cathodic sides, and the cathode further divided the cathodic side into catholyte and CO_2 gas chambers. Unless specified, both anolyte and catholyte were 1 M KOH aqueous solution. The working electrode was a catalyst-coated GDL with a geometric area of 1.5 cm^2. A mini-Ag/AgCl (1 mm, leak-free LF-1) and IrO_2-coated Titanium mesh were used as reference and counter electrodes, respectively. All reported potentials were rescaled to the reversible hydrogen electrode (RHE). The details of FE calculations for gaseous and liquid products are provided in the Supporting Information.

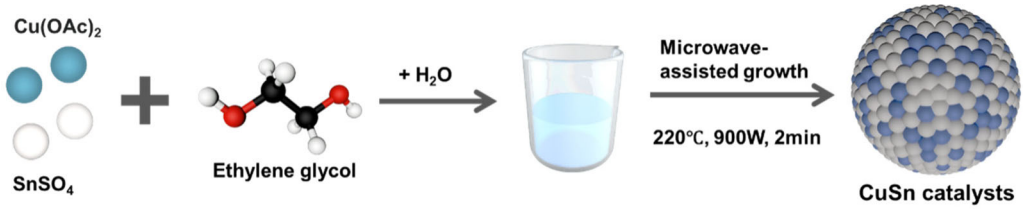

Scheme 1. Illustration of the synthesis process of CuSn catalysts.

3. Results and Discussion

3.1. Physicochemical Characterization of the As-Prepared Catalysts

The atomic ratios of Cu to Sn in the as-prepared bimetallic catalysts were analyzed by ICP-OES. As shown in Table S1, Supporting Information, the actual Cu:Sn ratios are 3.1, 1.9, and 0.53 for the Cu_8Sn_2, Cu_7Sn_3, and Cu_5Sn_5 samples, respectively. At lower Cu:Sn ratios, the actual values closely match the nominal ones, whereas at the highest ratio, the Cu content is significantly lower than expected.

FESEM was employed to investigate the morphological features of the as-prepared materials (**Figure 1**a–d). The Cu_2O sample consists of micrometer-sized cubic particles. Upon the addition of Sn, a significant morphological transformation is observed, independent of the Sn concentration. All CuSn catalysts exhibit similar morphology characterized by agglomerates of densely packed nanoparticles.

TEM analysis was performed on the selected Cu_5Sn_5 sample, confirming the agglomerations of very small nanoparticles with a broad distribution in size (about 2 to 7 nm in diameter). TEM images of the sample are shown in **Figure 2**a,c. Figure 2b reports the Fast Fourier transform (FFT) of the image in Figure 2a. These images demonstrate that the nanoparticles are crystalline, displaying lattice fringes with interplanar spacings predominantly of 0.33–0.34 nm, which can be indexed to the (110) planes of SnO_2. A minority of fringes with spacings of 0.25–0.26 nm are also observed, consistent with the (101) planes of SnO_2.[24] Figure 2d,e shows an EDX map of the sample acquired in scanning TEM (STEM mode), where the local abundance of Sn and Cu is displayed along with the high-angle annular dark-field (HAADF) image of the sample portion. These analyses show the presence of Cu and Sn all over the sample with a distribution not always uniform. While the main part of the agglomerations shows a homogeneous ratio of Sn and Cu, there are also a certain number of nanoparticles showing a higher fraction of Cu. Such particles are likely to be preferentially located on the outer surfaces of agglomerations.

Figure 3 presents the XRD patterns of all as-prepared catalysts. The Cu_2O sample displays diffraction peaks corresponding to the crystalline structure of cuprous oxide (Cu_2O, PDF #01-1142), with no detectable impurities. A similar pattern is observed for the Cu_8Sn_2 sample, showing no significant presence of crystalline Sn phases, as further confirmed by the higher-resolution plotting (Figure S2, Supporting Information). Increasing the Sn content in the Cu_7Sn_3 sample leads to the appearance of crystalline SnO_2 (PDF #01-0657) and metallic Cu (PDF #01-01241). In the Cu_5Sn_5 sample, which contains the highest Sn concentration, only peaks corresponding to SnO_2 and metallic Cu are observed. The broad peaks are attributed to the small crystallite size of SnO_2.[24]

Raman spectroscopy analysis was performed on selected samples, as displayed in **Figure 4**. The Raman spectrum of Cu_2O reveals its preliminary oxidation states, with a clear signature of Cu_2O as evidenced by the most prominent peak at 217 cm^{-1} and a further peak at 145 cm^{-1}. Weak signals from CuO are observed at 271 cm^{-1}, 332 cm^{-1}, and 611 cm^{-1}.[30,31] The small amount of CuO is attributed to surface oxidation upon air exposure, typically forming in an amorphous state or in quantities too low to be detected by XRD.[32,33] Raman spectrum of Cu_5Sn_5 sample shows a dominant feature at 611 cm^{-1} and some additional weaker features at 499 cm^{-1}, 535 cm^{-1}, 675 cm^{-1}, and

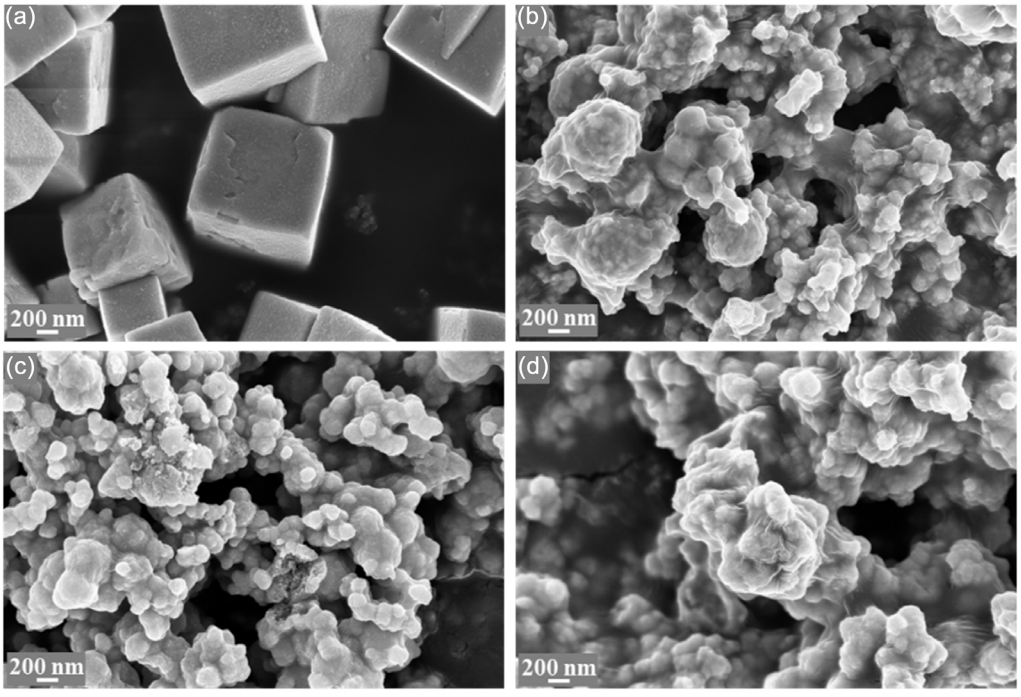

Figure 1. FESEM images of as-prepared catalysts. a) Cu_2O, b) Cu_8Sn_2, c) Cu_7Sn_3, and d) Cu_5Sn_5.

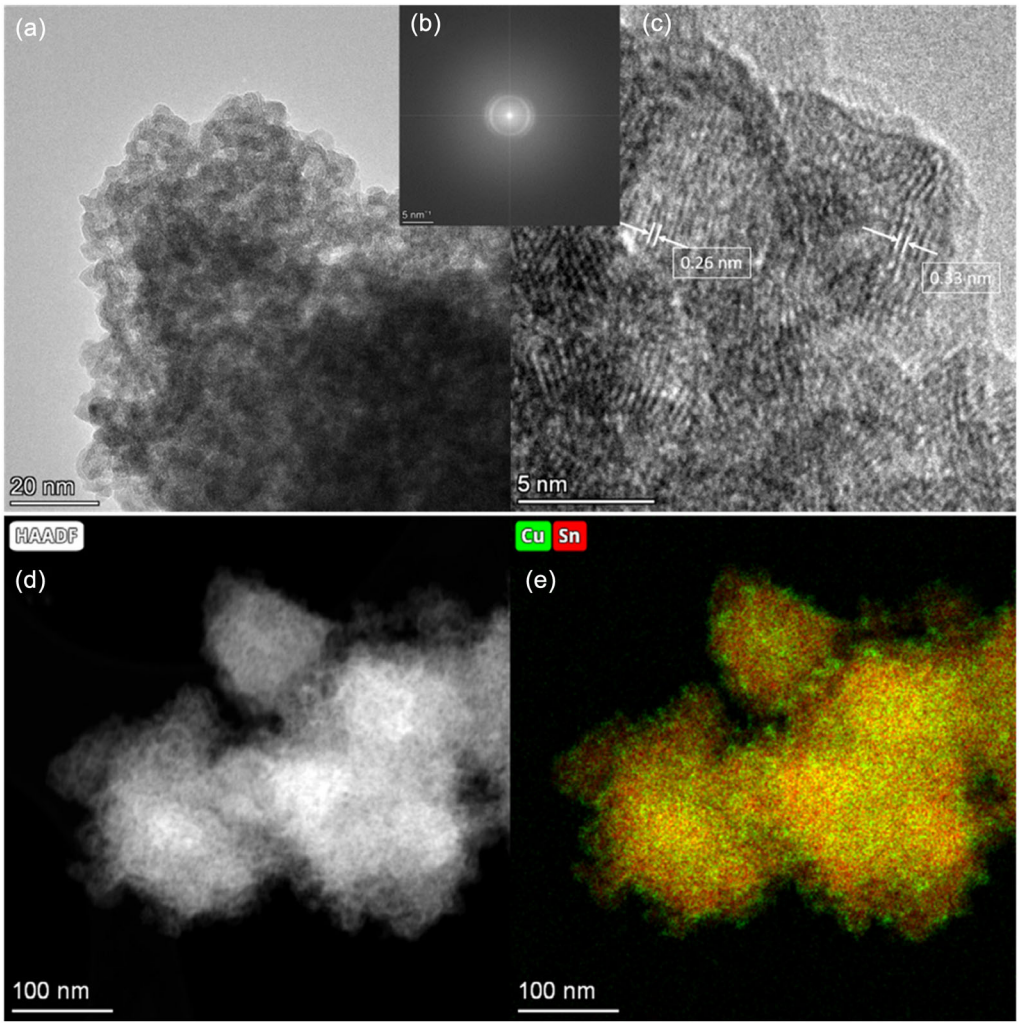

Figure 2. High-magnification TEM images of the compound Cu_5Sn_5. a) Zoomed view displaying the average size of particles in the agglomerates, b) FFT of the image reported in (a), c) magnified view showing the two lattice spacings which were found in the structure, d) HAADF-STEM image of and e) the relative abundance of Cu and Sn obtained by EDX analysis in the same area.

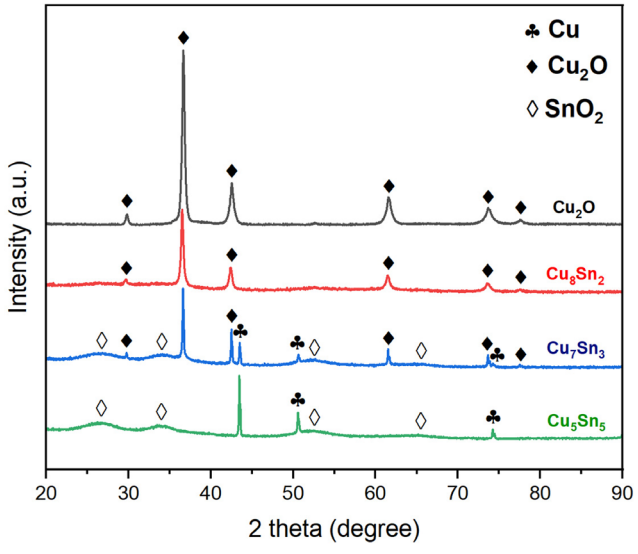

Figure 3. XRD patterns of synthesized catalysts.

745 cm^{-1}, which arise from the vibrations in SnO_2 nanocrystals with a shift related to the interaction of SnO_2 with CuO, in line with previously reported observations.[31,34] Both Cu_8Sn_2 and Cu_7Sn_3 catalysts show a surface composed of Cu oxides and SnO_2 (Figure S3, Supporting Information).

In summary, the CuSn samples exhibit similar morphologies to one another, but show notable differences compared to the Cu_2O sample. In contrast, their chemical composition is strongly influenced by the Cu-to-Sn ratio: increasing Sn content promotes the formation of SnO_2 and metallic Cu. Nonetheless, Cu and Sn are homogeneously distributed at the nanoscale, with only a slight enrichment of Cu at the edges.

3.2. Electrochemical Characterization

The catalytic performance toward the CO_2 RR of various CuSn electrodes was explored in 1 M KOH alkaline solution at a current density of -200 mA cm^{-2}. The Cu_2O electrode was also tested for

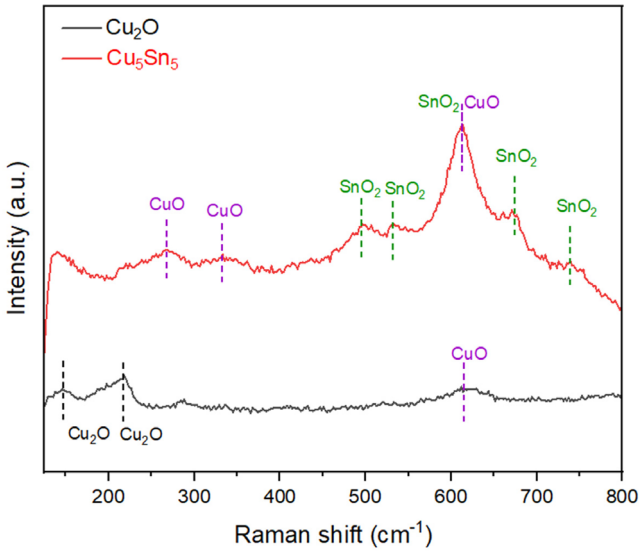

Figure 4. Raman spectra of synthesized Cu_2O and selected CuSn sample.

comparison. As shown in **Figure 5**a, the Cu_2O electrode mainly produces CO and C_2H_4, with a scarce selectivity of 6% for formate. In contrast, all CuSn electrodes exhibit a significantly enhanced selectivity toward formate production. The Cu_8Sn_2 sample shows a FE_{HCOO^-} of 55%, which further increases to 86% and 92% for Cu_7Sn_3 and Cu_5Sn_5, respectively. It is interesting to note that the potential follows a clear trend at the applied current density: $Cu_5Sn_5 > Cu_7Sn_3 > Cu_8Sn_2 > Cu_2O$, reflecting the same order in the catalytic activity of these electrodes. These results indicate that the addition of Sn plays a crucial role in shifting the selectivity of Cu toward formate production, and its concentration significantly influences the enhancement of formate formation. The enhanced performance observed in high Sn-loading samples could be attributed to a cooperative effect between metallic Cu and SnO_2, where metallic Cu enhances electron transfer,[32] while SnO_2-derived sites favor formate formation.[35,36]

The Cu_5Sn_5 bimetallic catalyst was further evaluated at current densities of -100 and $-300\ mA\ cm^{-2}$. As shown in **Figure 6**a, it maintains consistently high selectivity for formate across the tested current range, with faradaic efficiencies between 85% and 92%. Figure 6b shows that the potential remains nearly stable at each current density, with a gradual negative shift as the current increases, suggesting no significant mass transport limitations. The combination of high selectivity and relatively low overpotentials highlights the Cu_5Sn_5 catalyst as a highly promising candidate for CO_2-to-formate conversion.

The stability of the Cu_5Sn_5 catalyst was assessed through a long-term test in a flow cell using 1 M KOH electrolyte. As shown in **Figure 7**, the FE_{HCOO^-} remains above 80% during the first 5 h, followed by a gradual decline of ≈10% over the subsequent 15 h. The potential stays stable for 12 h before experiencing a gradual negative shift of about 200 mV. The decline in performance is likely due to a combination of factors and cannot be attributed to a single cause. However, since no backpressure was applied to the gas or liquid lines during the test, gradual electrode flooding over time is a plausible explanation. In any case, the observed stability is consistent with the best-performing systems reported in the literature under similar experimental conditions.[13,37]

In alkaline electrolytes, CO_2 reduction primarily yields formate rather than HCOOH, due to the high pH and the low pKa of HCOOH (3.75). As a result, an additional acidification step is required to convert formate into the more valuable HCOOH, increasing the overall process cost. Direct production of HCOOH requires acidic electrolytes (pH < 3). However, in such conditions, the hydrogen evolution reaction (HER) typically dominates due to the high proton concentration at the electrode/electrolyte interface, often suppressing CO_2RR.[38,39] Thus, the catalyst's selectivity plays a more critical role under acidic conditions. To evaluate the potential of Cu_5Sn_5 for direct HCOOH production, CO_2RR tests were conducted in 0.5 M K_2SO_4 (pH 3) using a flow cell. The acidic electrolyte was prepared by adding concentrated H_2SO_4 to a 0.5 M K_2SO_4 solution, maintaining a total K^+ concentration of ≈1.0 M. During testing, the catholyte was circulated in

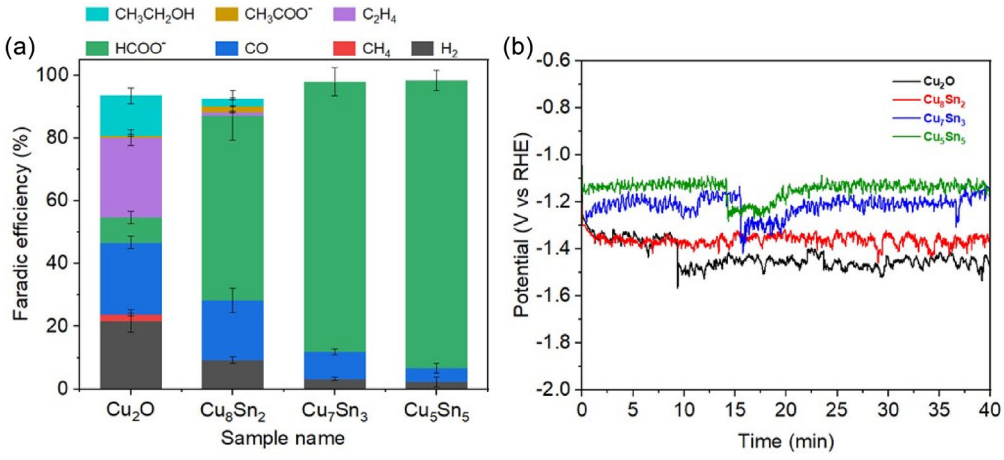

Figure 5. CO_2RR performance of various electrodes at $-200\ mA\ cm^{-2}$ in 1 M KOH. a) FEs of different products and b) corresponding chronopotentiometry curves.

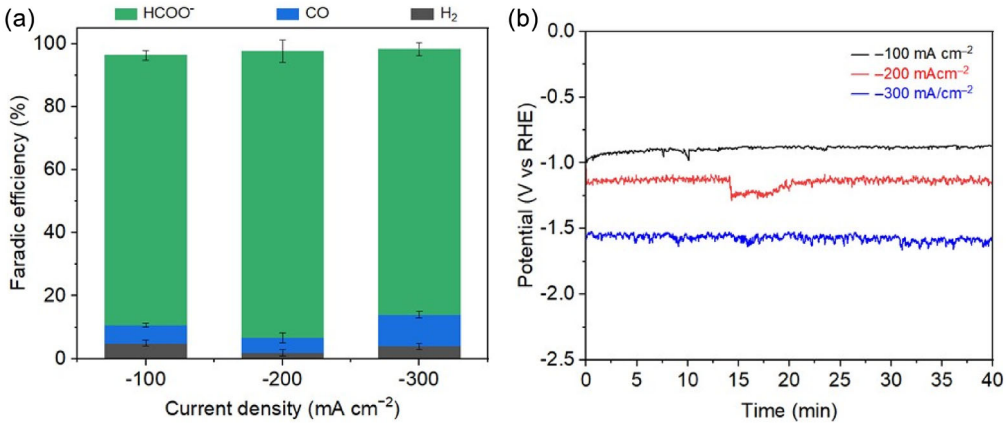

Figure 6. CO_2RR performance of Cu_5Sn_5 catalyst at different current densities in 1 M KOH. a) FEs of various products and b) corresponding chronopotentiometry curves.

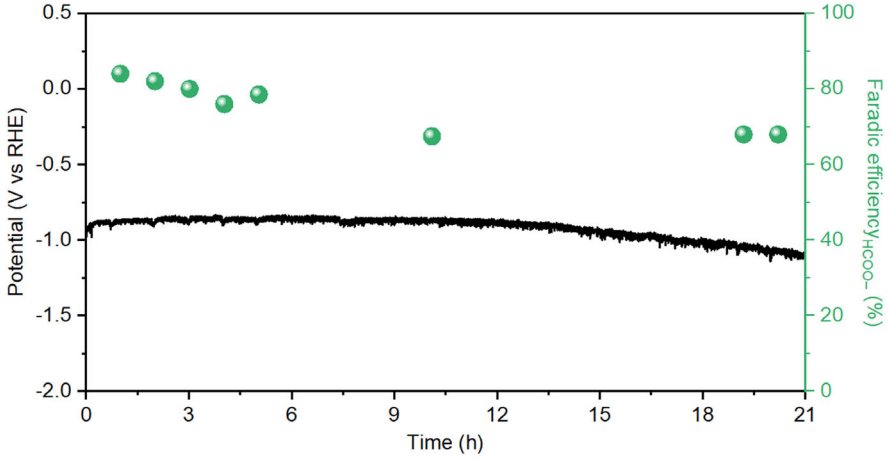

Figure 7. Long-term CO_2RR test on Cu_5Sn_5 electrode at $-100\ mA\ cm^{-2}$.

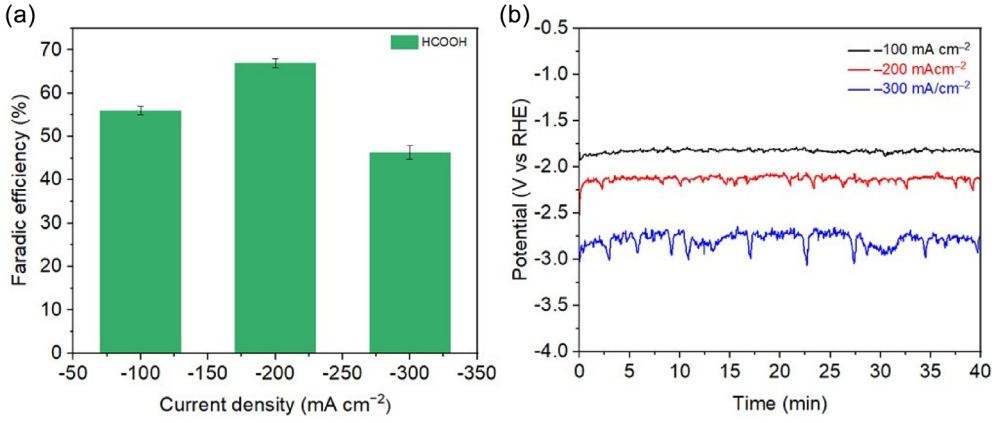

Figure 8. CO_2RR performance of Cu_5Sn_5 catalyst in 0.5 M K_2SO_4 (pH 3). a) FEs of HCOOH at various current densities and b) corresponding CO_2RR chronopotentiometry curves.

single-pass mode. As shown in **Figure 8**, the Cu_5Sn_5 electrode predominantly produces HCOOH across the tested current densities, reaching a peak FE of 70% at $-200\ mA\ cm^{-2}$. Compared to alkaline conditions, the acidic setup requires a more negative potential to reach the same current density, indicating that the CuSn electrode exhibits higher activity in a basic environment. To understand this phenomenon, the electric double layer capacitance (C_{dl}) of Cu_5Sn_5 electrodes after tests in pH 3 and 14 electrolytes was assessed. As illustrated in Figure S4, Supporting Information, the C_{dl} at pH 14 is 2.5 times as high as that at pH 3,

Table 1. Performance comparison of various electrocatalysts for CO_2RR to formate.

Catalyst	Electrolyte	j_{HCOO^-} [mA cm^{-2}]	Potential (V versus RHE)	FE_{HCOO^-} [%]	Reference
Cu_5Sn_5	1 M KOH	−184	−1.1	92	This work
Cu_5Sn_5	0.5 M K_2SO_4 (pH 3)	−140	−2.1	70	This work
Cu-SnS_2	0.5 M $KHCO_3$	−23.8	−1.0	90.5	[23]
5%Cu-SnO_2	0.5 M $KHCO_3$	−22	−0.9	91	[24]
Cu_3Sn/Cu_6Sn_5	1 M KOH	−18.9	−1.0	87	[25]
Hemicapsule Cu@SnO_2	0.1 M $KHCO_3$	−28	−1.35	67	[26]
CuSn NPs/C-A	0.1 M $KHCO_3$	−12.6	−1.0	71.5	[27]
CuS/SnO_2-S	0.5 M $KHCO_3$	−18.8	−0.8	84.9	[28]
CuO/SnO_2	1 M KOH	−3.19	−1.05	57.5	[40]
R-$CuSnO_3$	1 M KOH	−26	−0.9	93.4	[41]
CuO–SnO_2 NFs	1 M KOH	−186	−0.7	74.3	[42]
CuSn HFGDE	0.5 M $KHCO_3$	−68	−1.2	78	[43]
Cu–Sn aerogel	0.5 M $KHCO_3$	−21.8	−1.1	90.8	[44]

highlighting a significant enhancement in the electrochemically active surface area (ECSA) under alkaline conditions. A higher ECSA provides more active sites, thereby boosting the overall electrode activity in a basic electrolyte.

3.3. Comparison of Synthesized CuSn Catalysts with Literature

The catalyst proposed in this study shows superior activity and selectivity for formate production in CO_2RR compared to previously reported Cu- and Sn-based systems (**Table 1**). The Cu and Sn sources are low-cost and abundantly available. Moreover, the microwave-assisted one-pot synthesis is energy-efficient, rapid, and reproducible. These excellent performances highlight the strong potential of the proposed catalysts for practical applications.

4. Conclusion

This study presents CuSn bimetallic catalysts synthesized via a simple microwave-assisted method for the efficient electrochemical conversion of CO_2 to formate/formic acid. The catalyst morphology remains largely unchanged across different Sn contents, from 25 at% to 65 at%. However, the phase composition varies significantly with Sn content: the low-Sn sample predominantly exhibits crystalline Cu_2O, whereas the high-Sn sample shows crystalline phases of metallic Cu and SnO_2. These compositional differences strongly influence the selectivity of the CO_2 reduction reaction, highlighting the critical role of Sn content in tuning catalyst performance. Specifically, the high-Sn sample demonstrates excellent selectivity (92%) and good activity (−1.1 V versus RHE at −200 mA cm^{-2}) for formate production in alkaline conditions. This remarkable performance could be attributed to the synergistic interaction between metallic Cu and SnO_2, where the former facilitates electron transfer and the SnO_2-derived sites promote formate formation. Moreover, it maintains a promising selectivity of 70% for direct formic acid production in acidic electrolyte. This study offers a new pathway for developing high-performance and low-cost catalysts for industrial-scale CO_2 conversion into valuable chemical products.

Acknowledgements

This work is supported by the EU's Horizon 2021 programme under the Marie Skłodowska-Curie Doctoral Networks (MSCA-DN) (grant agreement no 101072830) and the National Recovery and Resilience Plan (NRRP) of Italian Ministry of Research (Project code: IR0000027, CUP: B33C22000710006, Project title: iENTRANCE). We thank Filippo Drago for the ICP-OES measurements.

Open access publishing facilitated by Istituto Italiano di Tecnologia, as part of the Wiley - CRUI-CARE agreement.

Conflict of Interest

The authors declare no conflict of interest.

Data Availability Statement

The data that support the findings of this study are available from the corresponding author upon reasonable request.

Keywords: bimetallic electrocatalysts · carbon dioxide conversion · formic acid · microwave-assisted synthesis · selectivity

[1] C. Oloman, H. Li, Electrochemical processing of carbon dioxide, *ChemSusChem* **2008**, *1*, 385.
[2] J. Qiao, Y. Liu, F. Hong, J. Zhang, A review of catalysts for the electroreduction of carbon dioxide to produce low-carbon fuels, *Chem. Soc. Rev.* **2013**, *43*, 631.
[3] Y. Chen, C. W. Li, M. Kanan, Aqueous CO_2 reduction at very low overpotential on oxide-derived Au nanoparticles, *J. Am. Chem. Soc.* **2012**, *134*, 19969.
[4] N. Han, Y. Wang, H. Yang, J. Deng, J. Wu, Y. Li, Y. Li, Ultrathin bismuth nanosheets from in situ topotactic transformation for selective electrocatalytic CO_2 reduction to formate, *Nat. Commun.* **2018**, *9*, 1320.

[5] S. Zhang, Q. Fan, X. Rong, T. J. Meyer, CO_2 reduction: from homogeneous to heterogeneous electrocatalysis, *Acc. Chem. Res.* **2022**, *53*, 255.
[6] D. Ren, Y. Deng, A. D. Handoko, C. S. Chen, S. Malkhandi, B. S. Yeo, Selective electrochemical reduction of carbon dioxide to ethylene and ethanol on Copper(I) oxide catalysts, *ACS Catal.* **2015**, *5*, 2814.
[7] M. Chen, S. Wan, Dynamic restructuring of Cu-Doped SnS_2 nanoflowers for highly selective electrochemical CO_2 reduction to formate, *Angew. Chem.* **2021**, *133*, 26737.
[8] M. G. Kibria, J. P. Edwards, C. M. Gabardo, C.-T. Dinh, A. Seifitokaldani, D. Sinton, E. H. Sargent, Electrochemical CO_2 reduction into chemical feedstocks: from mechanistic electrocatalysis models to system design, *Adv. Mater.* **2019**, *31*, 1807166.
[9] H. Shen, H. Jin, H. Li, H. Wang, J. Duan, Y. Jiao, S. Qiao, Acidic CO_2-to-HCOOH electrolysis with industrial-level current on phase engineered tin sulfide, *Nat. Commun.* **2023**, *14*, 2843.
[10] Z. Kuang, W. Zhao, C. Peng, Q. Zhang, Y. Xue, Z. Li, H. Yao, X. Zhou, H. Chen, Hierarchically porous SnO_2 coupled organic carbon for CO_2 electroreduction, *ChemSusChem* **2020**, *13*, 5896.
[11] X. Zhu, Y. Xu, L. Ran, S. Chen, X. Qiu, Three-dimensional porous indium single-atom catalysts with improved accessibility for CO_2 reduction to formate, *Inorg. Chem.* **2024**, *63*, 3893.
[12] J. Zeng, N. B. D. Monti, T. Chen, M. Castellino, W. Ju, M. A. O. Lourenço, P. Jagdale, C. F. Pirri, Evolution of bismuth electrodes activating electrosynthesis of formate from carbon dioxide reduction, *Catal. Today* **2024**, *437*, 114743.
[13] N. B. D. Monti, T. Chen, L. Huang, J. Wang, M. Fontana, C. F. Pirri, W. Ju, J. Zeng, Unveiling the origin of pH-dependent catalytic performance of Bi_2O_3 nanostructure for electrochemical CO_2 reduction, *J. Phys. Chem. Lett.* **2025**, *16*, 3761.
[14] J. Du, Y. Xin, M. Dong, J. Yang, Q. Xu, H. Liu, B. Han, Copper/Carbon heterogenous interfaces for enhanced selective electrocatalytic reduction of CO_2 to formate, *Small* **2021**, *17* (41)2102629.
[15] J. Zhang, Y. Chen, F. Xu, Y. Zhang, J. Tian, Y. Guo, G. Chen, X. Wang, L. Yang, Q. Wu, Z. Hu, High-dispersive Pd nanoparticles on hierarchical N-Doped carbon nanocages to boost electrochemical CO_2 reduction to formate at low potential, *Small* **2023**, *19*, 2301577.
[16] F. Li, L. Chen, M. Xue, T. Williams, Y. Zhang, D. R. MacFarlane, J. Zhang, Towards a better Sn: efficient electrocatalytic reduction of CO_2 to formate by Sn/SnS_2 derived from SnS_2 nanosheets, *Nano Energy* **2017**, *31*, 270.
[17] F. Li, L. Chen, G. P. Knowles, D. R. MacFarlane, J. Zhang, Hierarchical mesoporous SnO_2 Nanosheets on carbon cloth: a robust and flexible electrocatalyst for CO_2 reduction with high efficiency and selectivity, *Angew. Chem. Int. Ed.* **2017**, *56*, 505.
[18] Y. Qian, Y. Liu, H. Tang, B.-L. Lin, Highly efficient electroreduction of CO_2 to formate by nanorod@2D nanosheets SnO, *J. CO_2 Util.* **2020**, *42*, 101287.
[19] S. You, J. Xiao, S. Liang, W. Xie, T. Zhang, M. Li, Z. Zhong, Q. Wang, H. He, Doping engineering of Cu-based catalysts for electrocatalytic CO_2 reduction to multi-carbon products, *Energy Environ. Sci.* **2024**, *17*, 5795.
[20] X. He, L. Lin, X. Li, M. Zhu, Q. Zhang, S. Xie, B. Mei, F. Sun, Z. Jiang, J. Cheng, Y. Wang, Roles of Copper(I) in water-promoted CO_2 electrolysis to multicarbon compounds, *Nat. Commun.* **2024**, *15*, 9923.
[21] Y. Zhao, Y. Wang, Z. Yu, C. Song, J. Wang, H. Huang, L. Meng, M. Liu, L. Liu, Gold single atom doped defective nanoporous copper octahedrons for electrocatalytic reduction of carbon dioxide to ethylene, *ACS Nano* **2025**, *19*, 4505.
[22] J. Yu, J. Wang, Y. Ma, J. Zhou, Y. Wang, P. Lu, J. Yin, R. Ye, Z. Zhu, Z. Fan, Recent progresses in electrochemical carbon dioxide reduction on copper-based catalysts toward multicarbon products, *Adv. Funct. Mater.* **2021**, *31*, 2102151.
[23] M. Chen, S. Wan, L. Zhong, D. Liu, H. Yang, C. Li, Z. Huang, C. Liu, J. Chen, H. Pan, D.-S. Li, S. Li, Q. Yan, B. Liu, Dynamic restructuring of Cu-Doped SnS_2 nanoflowers for highly selective electrochemical CO_2 reduction to formate, *Angew. Chem.* **2021**, *133*, 26437.
[24] B. Li, J. Chen, L. Wang, D. Xia, S. Mao, L. Xi, S. Ying, H. Zhang, Y. Wang, Dynamic reconstruction of Cu-Doped SnO_2 for efficient electrochemical reduction of CO_2 to formate, *Appl. Catal. B: Environ. Energy* **2025**, *363*, 124784.
[25] J. Wang, J. Zou, X. Hu, S. Ning, X. Wang, X. Kang, S. Chen, Heterostructured intermetallic CuSn catalysts: high performance towards the electrochemical reduction of CO_2 to formate, *J. Mater. Chem. A* **2019**, *7*, 27514.
[26] P.-F. Yin, J. Fu, Q. Yun, B. Chen, G. Liu, L. Li, Z. Huang, Y. Ge, H. Zhang, Preparation of amorphous SnO_2-encapsulated multiphased crystalline Cu heterostructures for highly efficient CO_2 reduction, *Adv. Mater.* **2022**, *34*, 2201114.
[27] P. Wang, M. Qiao, Q. Shao, Y. Pi, X. Zhu, Y. Li, X. Huang, Phase and structure engineering of copper tin heterostructures for efficient electrochemical carbon dioxide reduction, *Nat. Commun.* **2018**, *9*, 4933.
[28] T. Dou, J. He, S. Diao, Y. Wang, X. Zhao, F. Zhang, X. Lei, Dynamic reconstructuring of CuS/SnO_2-S for promoting CO_2 electroreduction to formate, *J. Energy Chem.* **2023**, *82*, 497.
[29] T. Gunji, H. Ochiai, Y. Isawa, Y. Liu, F. Nomura, M. Miyauchi, F. Matsumoto, Electrocatalytic conversion of carbon dioxide to formic acid over nanosized Cu6Sn5 intermetallic compounds with a SnO_2 shell layer, *Catal. Sci. Technol.* **2019**, *9*, 6577.
[30] M. Valvo, J. Thyr, T. Edvinsson, Defect-induced Raman scattering in Cu_2O nanostructures and their photocatalytic performance, *ChemElectroChem* **2023**, *10*, e202300376.
[31] X.-J. Zheng, Y.-J. Wei, L.-F. Wei, B. Xie, M.-B. Wei, Photocatalytic H_2 production from acetic acid solution over CuO/SnO_2 nanocomposites under UV irradiation, *Int. J. Hydrogen Energy* **2010**, *35*, 11709.
[32] J. Zeng, T. Rino, K. Bejtka, M. Castellino, A. Sacco, M. A. Farkhondehfal, A. Chiodoni, F. Drago, C. F. Pirri, Coupled copper–zinc catalysts for electrochemical reduction of carbon dioxide, *ChemSusChem* **2020**, *13*, 4128.
[33] J. Zeng, M. R. Fiorentin, M. Fontana, M. Castellino, F. Risplendi, A. Sacco, G. Cicero, M. A. Farkhondehfal, F. Drago, C. F. Pirri, Novel insights into Sb-Cu catalysts for electrochemical reduction of CO_2, *Appl. Catal. B: Environ.* **2022**, *306*, 121089.
[34] R. N. Mariammal, K. Ramachandran, B. Renganathan, D. Sastikumar, On the enhancement of ethanol sensing by CuO modified SnO_2 nanoparticles using fiber-optic sensor, *Sens. Actuators B* **2012**, *169*, 199.
[35] K. Bejtka, J. Zeng, A. Sacco, M. Castellino, S. Hernández, M. A. Farkhondehfal, U. Savino, S. Ansaloni, C. F. Pirri, A. Chiodoni, Chainlike mesoporous SnO_2 as a well-performing catalyst for electrochemical CO_2 reduction, *ACS Appl. Energy Mater.* **2019**, *2*, 3081.
[36] N. B. D. Monti, J. Zeng, M. Castellino, S. Porro, M. Bagheri, C. F. Pirri, A. Chiodoni, K. Bejtka, Effects of annealing conditions on the catalytic performance of anodized tin oxide for electrochemical carbon dioxide reduction, *Nanomaterials* **2025**, *15*, 121.
[37] N. B. D. Monti, G. A. El-Nagar, M. Fontana, F. Di Costola, S. Gupta, M. T. Mayer, C. F. Pirri, J. Zeng, Insights into the stability of copper gas diffusion electrodes for carbon dioxide reduction at high reaction rates, *Mater. Today Sustainability* **2025**, *30*, 101124.
[38] L.-P. Chi, Z.-Z. Niu, Y.-C. Zhang, X.-L. Zhang, J. Liao, Z.-Z. Wu, P.-C. Yu, M.-H. Fan, K.-B. Tang, M.-R. Gao, Efficient and stable acidic CO_2 electrolysis to formic acid by a reservoir structure design, *Proc. Natl Acad. Sci.* **2023**, *120*, e2312876120.
[39] Y. Jiang, L. Huang, C. Chen, Y. Zheng, S.-Z. Qiao, Catalyst–electrolyte interface engineering propels progress in acidic CO_2 electroreduction, *Energy Environ. Sci.* **2025**, *18*, 2025.
[40] M. Wang, H. Chen, M. Wang, J. Wang, Y. Tuo, W. Li, S. Zhou, L. Kong, G. Liu, L. Jiang, G. Wang, Tuning C1/C2 selectivity of CO_2 electrochemical reduction over in-situ evolved CuO/SnO_2 heterostructure, *Angew. Chem. Int. Ed.* **2023**, *62*, e202306456.
[41] T. Fan, J. Zhang, X. Zhang, M. Wang, X. Yi, Y. Lum, Z. Chen, Interface-stabilized high-valent Sn enables efficient CO_2 electroreduction to formate/formic acid across the full pH range, *Nano Energy* **2024**, *130*, 110135.
[42] S. Go, W. Kwon, D. Hong, T. Lee, S.-H. Oh, D. Bae, J.-H. Kim, S. Lim, Y.-C. Joo, D.-H. Nam, Thermodynamic phase control of Cu–Sn alloy electrocatalysts for selective CO_2 reduction, *Nanoscale Horizons* **2024**, *9*, 2295.
[43] H. Rabiee, X. Zhang, L. Ge, S. Hu, M. Li, S. Smart, Z. Zhu, Z. Yuan, Tuning the product selectivity of the Cu hollow fiber gas diffusion electrode for efficient CO_2 reduction to formate by controlled surface Sn electrodeposition, *ACS Appl. Mater. Interfaces* **2020**, *12*, 21670.
[44] B. Ren, J. Shao, H. Li, Q. Xu, Copper–Tin bimetallic aerogel alloy for the electroreduction of CO_2 to formate, *New J. Chem.* **2025**, *49*, 2201.

Manuscript received: July 31, 2025
Revised manuscript received: October 1, 2025
Version of record online: November 3, 2025